

## CHAPTER IV

### Probing adsorbate oscillation on metal surfaces

To date, studying molecular oscillations on metal surfaces has mainly been done in the energy domain. In order to measure vibrational modes of molecules adsorbed on metal surfaces, energy loss techniques are typically used. In general, electron energy loss spectroscopy (EELS) is commonly used to measure the vibrational energies of normal modes in the higher energy range; for low energy modes, the technique of helium atom scattering is used instead because the high mass of the helium atom helps to resolve the small energy loss resulting from the scattering process. These techniques have successfully measured the vibrational frequencies of adsorbates, i.e. the metal-adsorbate vibrational mode energies and frustrated rotational mode energies, etc. However, it is not possible using these techniques to measure instantaneous excitation/de-excitation processes as a result of external “triggers” to molecules. For example, when a laser pulse irradiates molecules deposited on a metal surface, vibrational modes of the adsorbates can be triggered either due to the traditional phonon-induced (cw or nanosecond pulses), or hot surface electron-induced (femtosecond pulses) excitation. Moreover, it is unlikely that scattering experiments can measure how long the adsorbates will take for the vibrational process to start

after the excitation, and the time scale of the corresponding damping process. Therefore, time-domain measurements are needed as a complement to scattering experiment in order to reveal more information about dynamics.

Molecular vibrations are also very important for surface chemical reactions where molecules approach each other to react through various degree of vibrational motions, and electronic rearrangements. Therefore, in order to better understand some of the underlying mechanisms of surface chemistry, time-domain techniques are necessary to follow reactions at the molecular level in a step-by-step fashion.

Currently, time domain measurements are still very difficult due to a lack of appropriate techniques with both high surface sensitivity and high time-resolution (fs). In this chapter, we will demonstrate that by using the TR-UPS technique, and by varying the polarization of the incoming EUV probe pulses, it is possible to measure the vibrational frequencies of adsorbates on metal surfaces.

#### **4.1 Photoelectric current affects by molecular symmetry and EUV polarization**

In photoemission spectroscopy (PES), the transition probability of the photoelectric current produced in the PES process results from the excitation of electrons from an initial state with wavefunction  $\psi_i$  to a final state with wavefunction  $\psi_f$  by a photon field having the vector potential  $\vec{A}$  ( the direction of  $\vec{A}$  is the same as the polarization  $\vec{E}$  of the laser field). Hence, the transition probability (or photoelectron emission probability)  $w$  can be formulated using the Fermi-Golden Rule (or the first Born approximation) which assumes that the wavelength of the radiation is large compared to the dimensions of the excitation

volume [92],

$$w \propto \frac{2\pi}{\hbar} |\langle \psi_f | \hat{\mu} | \psi_i \rangle|^2 \delta(E_f - E_i - \hbar\omega) \quad (4.1)$$

where  $\hat{\mu} = e\vec{r}$  is the permanent electric dipole moment and  $\vec{r}$  has the same direction of the polarization of the laser field  $\vec{E}$ . Certain assumptions about the wavefunctions  $\psi_i$  and  $\psi_f$  can be legitimately applied in our case to simplify the transition matrix element  $\langle \psi_f | \hat{\mu} | \psi_i \rangle$ . The two wavefunctions ( $\psi_i$  and  $\psi_f$ ) here are the full wavefunctions describing all the electrons in the system, and hence Eq. 4.1 is an equation for the many-body problem. For the first approximation, we can simplify this complicated many-body equation to a simple “one-electron” equation by neglecting effects caused by other electrons. The simplification for the initial and final state wavefunctions is explained in the following. For the final state, the adsorbate molecule is in the excited state with one less electron in the atomic core, plus a free electron with kinetic energy  $E_{kin}$ . Therefore, it is reasonable to approximate the initial-state wavefunction as a product of the single electron orbital  $\phi_{i,k}$ , from which the electron  $k$  will be excited, and write the wavefunction of the remaining electrons as  $\psi_{i,R}^k(N-1)$ , for the atom with  $N$  total electrons. Therefore, the initial-state wavefunction can be simplified to be –

$$\psi_i(N) = C \phi_{i,k} \psi_{i,R}^k(N-1) \quad (4.2)$$

where  $C$  is the normalization constant. By following this line of thought, the final state wavefunction  $\psi_f$  can also be simplified as a product of single-electron wavefunctions  $\phi_{f,E_{kin}}$  of the photoemitted free electron and the remaining  $(N-1)$  electron wavefunctions  $\psi_{f,R}^k(N-1)$ ,

$$\psi_f(N) = C \phi_{f,E_{kin}} \psi_{f,R}^k(N-1) \quad (4.3)$$

Therefore, the transition matrix element of Eq. 4.1 can be separated into two terms,

$$\langle \psi_f | \hat{\mu} | \psi_i \rangle = \langle \phi_f | \hat{\mu} | \phi_i \rangle \langle \psi_{f,R}^k(N-1) | \psi_{i,R}^k(N-1) \rangle \quad (4.4)$$

The first term is the one-electron matrix element, and the second term is the  $(N-1)$  electron overlap integral. The second term generally accounts for many other features in the photoemission spectrum, such as the core-level shifts and satellite peaks [92, 93], which are not considered here. Therefore, one can approximate that the remaining orbitals of the initial-state  $\psi_{i,R}^k(N-1)$ , and the final-state  $\psi_{f,R}^k(N-1)$  to be identical. This approximation is often called the “frozen-orbital approximation”, causing the second term to be approximated as  $\langle \psi_{f,R}^k(N-1) | \psi_{i,R}^k(N-1) \rangle \approx 1$ . The total transition matrix element now becomes very simple and results in a one-electron matrix element –

$$w \propto \langle \phi_f | \hat{\mu} | \phi_i \rangle \propto \langle \phi_f | \vec{r} | \phi_i \rangle \quad (4.5)$$

Since the photoelectric current measured by detectors is directly proportional to the photoelectron emission probability  $w$ , according to Eq. 4.5, the photoemission current is simply proportional to the integration of the single-electron wavefunctions of the initial orbital  $\phi_i$  and the final free electron wavefunction  $\phi_f$ , with the polarization of the applied electric field  $\vec{r}$ .

In this experiment, CO molecules are adsorbed on a platinum(111) surface, where CO is known to adsorb in the upright position (see next section). The CO molecule is a linear molecule and belongs to the symmetry point group of  $C_{\infty v}$ . The corresponding character table of the point group  $C_{\infty v}$  is tabulated in Table 4.1. According to Eq. 4.5 and by using the terminology of group theory, for a given polarization  $\vec{E}$ , the photoelectron emission

$C_{\infty v}$	$E$	$2C_{\infty}^{\phi}$	$2C_{\infty}^{2\phi}$	$2C_{\infty}^{3\phi}$	$\dots$	$\infty\sigma_v$	
$A_1 \equiv \Sigma^+$	1	1	1	1	$\dots$	1	$z$
$A_2 \equiv \Sigma^-$	1	1	1	1	$\dots$	-1	$R_z$
$E_1 \equiv \Pi$	2	$2 \cos(\phi)$	$2 \cos(2\phi)$	$2 \cos(3\phi)$	$\dots$	0	$(x, y), (R_x, R_y)$
$E_2 \equiv \Delta$	2	$2 \cos(2\phi)$	$2 \cos(4\phi)$	$2 \cos(6\phi)$	$\dots$	0	
$E_3 \equiv \Phi$	2	$2 \cos(3\phi)$	$2 \cos(6\phi)$	$2 \cos(9\phi)$	$\dots$	0	
$E_4 \equiv \Gamma$	2	$2 \cos(4\phi)$	$2 \cos(8\phi)$	$2 \cos(12\phi)$	$\dots$	0	
$\vdots$					$\vdots$		
$\Gamma_{x,y,z}$	3	$1 + 2 \cos(\phi)$	$1 + 2 \cos(2\phi)$	$1 + 2 \cos(3\phi)$	$\dots$	1	

Table 4.1: Character table of the symmetry group  $C_{\infty v}$ . ( $z$  is the direction of the principle symmetric axis)

probability  $w \neq 0$  only when the direct product of the irreducible representations of the three functions ( $\phi_i$ ,  $\phi_f$ , and  $\vec{r}$ ) contains the totally symmetric irreducible representation<sup>1</sup> ( $\Sigma^+$  in the case of  $C_{\infty v}$ ) [94]. Mathematically,

$$\Gamma_{\phi_i} \otimes \Gamma_{\vec{r}} \otimes \Gamma_{\phi_f} \ni \Sigma^+ \quad (4.6)$$

or equivalently [95],

$$\Gamma_{\phi_i} \otimes \Gamma_{\vec{r}} = \Gamma_{\phi_f} \quad (4.7)$$

where  $\Gamma_{\phi_i}$  denotes the irreducible representation of the function  $i$ . For normal emission of the photoelectrons, the emission direction is along the principle symmetric axis  $z$ , which corresponds to the irreducible representation  $\Sigma^+$ , according to Table 4.1. Since irreducible representation  $\Sigma^+$  is totally symmetric, this simplifies Eq. 4.6 that  $w \neq 0$  if the direct products of the  $\Gamma_{\phi_i} \otimes \Gamma_{\vec{r}}$  contains  $\Sigma^+$ .

The polarization of the EUV probe pulses then affects the symmetry of  $\Gamma_{\vec{r}}$ . According to Table 4.1, for  $p$ -polarized EUV pulses, where the polarization of the pulses is parallel to the plane of incidence ( $z$  in the character table),  $\Gamma_{\vec{r}} = \Sigma^+$ . For  $s$ -polarized EUV

<sup>1</sup>An irreducible representation is a totally symmetric irreducible representation when the characters for all symmetric operations is equal to 1.

$C_{\infty v}$	$\Sigma^+$	$\Sigma^-$	$\Pi$	$\Delta$	$\Phi$	$\Gamma$	...
$\Sigma^+$	$\Sigma^+$	$\Sigma^-$	$\Pi$	$\Delta$	$\Phi$	$\Gamma$	
$\Sigma^-$		$\Sigma^+$	$\Pi$	$\Delta$	$\Phi$	$\Gamma$	
$\Pi$			$\Sigma^+ + [\Sigma^-] + \Delta$	$\Pi + \Phi$	$\Delta + \Gamma$	$\Phi + \text{H}$	
$\Delta$				$\Sigma^+ + [\Sigma^-] + \Gamma$	$\Pi + \text{H}$	$\Delta + \text{I}$	
$\Phi$					$\Sigma^+ + [\Sigma^-] + \text{I}$	$\Pi + \Theta$	
$\Gamma$						$\Sigma^+ + [\Sigma^-] + \text{K}$	
$\vdots$							

Table 4.2: Table of the direct product ( $\otimes$ ) of the symmetry group  $C_{\infty v}$

pulses, the polarization of the pulses is perpendicular to the plane of the incidence ( $x$  or  $y$  in the character table) and  $\Gamma_{\vec{r}} = \Pi$ . Table 4.2 is the direct product table for the symmetry group  $C_{\infty v}$ . According to this table, for an orbital with  $\sigma$  symmetry ( $\Gamma_{\phi_i} = \Sigma^+$ ),  $p$ -polarized EUV pulses ( $\Gamma_{\phi_r} = \Sigma^+$ ) are needed to have a non-zero photoelectron emission probability ( $\Sigma^+ \otimes \Sigma^+ = \Sigma^+$ ). On the other hand, for an orbital with  $\pi$  symmetry ( $\Gamma_{\phi_i} = \Pi$ ),  $s$ -polarized EUV pulses ( $\Gamma_{\phi_r} = \Pi$ ) are required ( $\Pi \otimes \Pi = \Sigma^+ + [\Sigma^-] + \Delta$  contains  $\Sigma^+$ ). Therefore, by changing the polarization of the EUV pulses, molecular orbitals with different symmetries can be selectively enhanced or suppressed in the photoemission spectrum. More detail discussion about the relation between the angular pattern of emitted photoelectrons and the laser polarization can be found in Ref. [95].

## 4.2 Symmetry of the orbitals of CO/Pt(111)

As mentioned in the previous paragraphs, CO is adsorbed on the Pt(111) surface for this experiment. The platinum surface is routinely cleaned with argon sputtering and oxygen annealing. After the platinum surface is cleaned, 5 L of CO is introduced onto the surface through a gas doser to achieve a saturation CO coverage of 0.5 ML. At this coverage, the CO molecules equally occupy the bridge  $\nu_b(\text{C} - \text{O}) = 232$  meV and atop sites

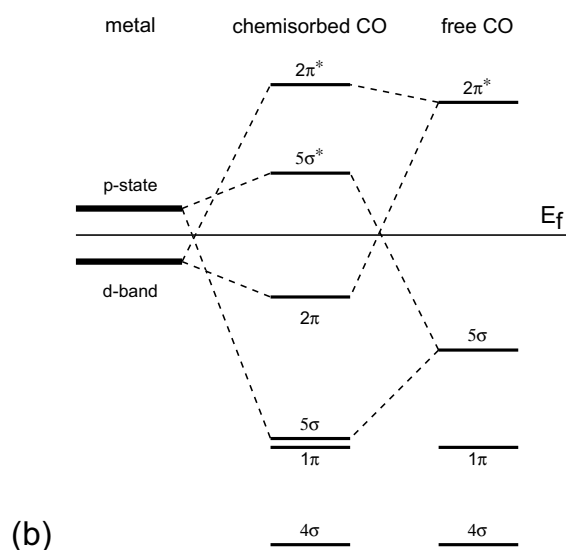
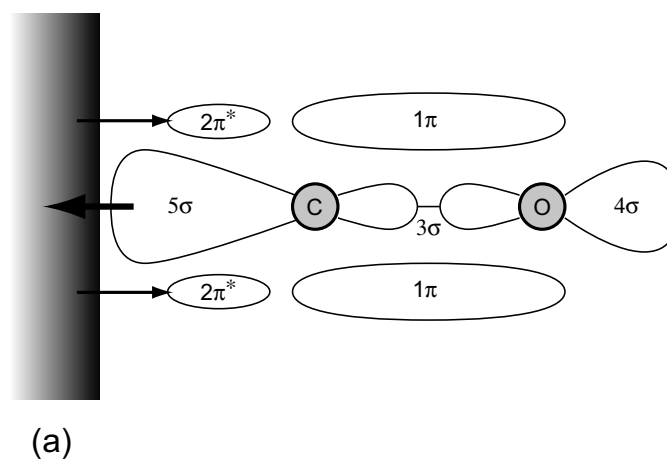


Figure 4.1: Schematic diagram showing the bonding character of a CO molecule adsorbed on a metal surface. (a) The CO-metal bond is provided by the most extended orbital of the molecule which is the  $5\sigma$  orbital. Charge back donation from the metal into the formerly empty  $2\pi^*$  orbitals is indicated by thin arrows. (b) Schematic energy level diagram of the CO-metal system. The energy levels on both sides are for the isolated CO molecule and the metal surface. The middle diagram illustrates the energy levels of an adsorbed CO molecule. Band splitting for the adsorbed CO happens for the  $5\sigma$  and  $2\pi^*$  levels due to hybridization with the metal  $d$ -band and the  $p$ -orbitals. (figures reproduced from Ref. [92])

$\nu_t(\text{C} - \text{O}) = 258 \text{ meV}$ , producing a  $c(4 \times 2)$  LEED pattern [75, 13]. The CO molecules adsorb in an upright position with the intermolecular axis perpendicular to the metal surface, with the carbon atom at the bottom bonded to the metal surface, while the oxygen atom resides on top. Figure 4.1(a) illustrates the outermost molecular orbitals of the CO molecule and indicates how the CO molecule binds to the platinum surface. The energetically highest occupied orbital and thus also the spatially most extended one is the  $5\sigma$  orbital which is located mainly on the carbon atom. Therefore, it is intuitively reasonable that the CO molecule tries to attach its “softest” part to the metal surface in the surface chemical bond. The initial step in binding is therefore a  $5\sigma$ -to-metal charge transfer. This charge transfer is compensated partly by back donation of charge from the metal surface onto the CO molecule. This back donated charge is into an orbital that is a mixture of the  $2\pi^*$  of the free CO molecule with the metal  $d$ -band [96]. It is interesting to note that in the free CO molecule, the  $2\pi^*$  orbital is about 1.5 eV above the vacuum level  $E_v$ , and the hybridization with the metal  $d$ -band causes it to locate below  $E_v$  [97].

Figure 4.1(b) illustrates the energy levels of the orbitals for free CO molecules and chemisorbed CO molecules on metal surfaces. When CO molecules are brought into contact with a metal surface, the  $5\sigma$  orbital of the CO molecule interacts with the  $p$ -orbital of the metal atoms, splitting the  $5\sigma$  orbital into a bonding and an anti-bonding state. The resulting bonding state is energetically only slightly higher than  $1\pi$  orbital, in contrast to its much higher energy position originally. The  $2\pi^*$  orbital also interacts with the  $d$ -band causing a splitting into a bonding and an anti-bonding state. The bonding state is located well below the Fermi-edge  $E_f$  in energy, and hence provides a back donation channel for

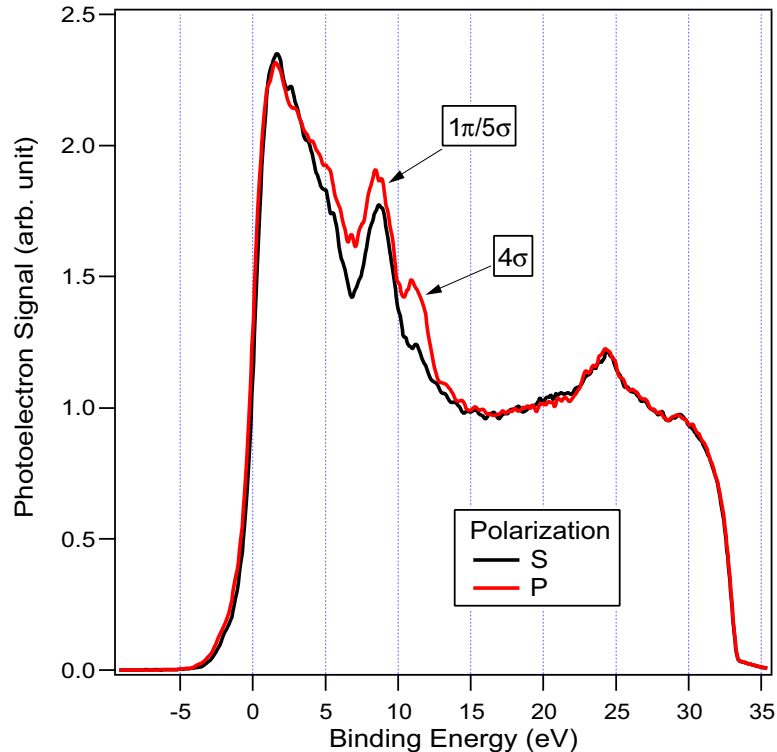


Figure 4.2: Photoemission spectrum of CO molecules adsorbed on a platinum(111) single crystal surface. Spectra are taken with high harmonic photons (42 eV) with different  $s$  (black) and  $p$  (red) polarizations.

charge transferring from platinum to the CO molecule.

As pointed out in the previous section, the orbital symmetry of the CO molecules results in different photoemission cross-sections depending on the polarization of the exciting EUV light. Figure 4.2 plots the photoemission spectra of CO on Pt(111) using  $s$  and  $p$  polarized EUV probe pulses without pump beam excitation, i.e. the so-called “static” spectra. The two spectra show significant similarities in both the high and low binding energy regions. However, in the energy range from 5 to 15 eV, noticeable differences are caused by the different polarizations of the EUV probe pulses. Comparing with the energy level diagram of the chemisorbed CO on Fig. 4.1(b), the peak at 9 eV binding energy can be assigned to the  $1\pi/5\sigma$  orbital combination – the energy lowering of the  $5\sigma$

orbital caused by hybridization with the metal  $d$ -band, results in a  $5\sigma$  bonding state that is indistinguishable with the  $1\pi$  orbital in energy. As shown in Fig. 4.2, there are changes in intensity for the  $1\pi/5\sigma$  peak when using different EUV polarizations. However, since the  $1\pi$  and the  $5\sigma$  orbitals are so close in energy after adsorption, it is difficult to use this peak to analyze the CO orientation.

There is another peak at a 12 eV binding energy that can be assigned to the  $4\sigma$  orbital. It has very different emission cross-sections for the two different EUV polarizations. As shown in Fig. 4.2, the  $4\sigma$  peak is greatly suppressed for  $s$ -polarized light, as expected due to the symmetry selection rule explained in the previous section. This kind of complementary behavior of  $\sigma$  and  $\pi$  emissions was first observed by Plummer *et al.* for CO/Ni(111) [98] and has been used to determine the geometry of the adsorbed molecules on metal surfaces [95]. There is still a little remnant of the  $4\sigma$  peak in the case of  $s$ -polarized light. This is because the TOF detector is mounted about  $30^\circ$  off the surface normal. Although the ideal case would be to mount the TOF detector normal to the sample, the off-normal mounting has a negligible effect on the photoemission yield for the  $4\sigma$  peak and therefore does not affect the overall experiment.

### 4.3 Resolving oscillations of adsorbed CO molecules

In the previous sections, it has been shown that there is a dependence of the photoelectron emission cross-section on the EUV polarization. Therefore, it is possible to use this property to measure the oscillation period of the adsorbate after excitation by an ultrafast pulse. After the surface is excited by an ultrafast pulse, hot electron tunneling from the substrate to the adsorbate can occur. The excited electrons raise the potential energy surface

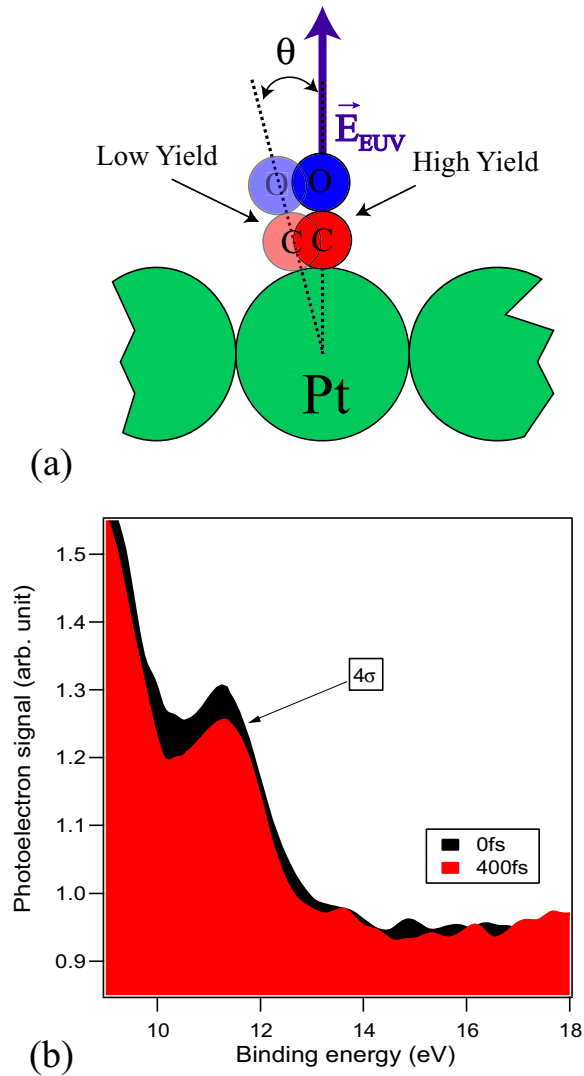


Figure 4.3: (a) Schematic diagram illustrating that when the CO molecules are aligned with the polarization of the EUV pulse, the photoemission cross-section is maximized. After excitation by an ultrafast laser pulse, the CO molecules start to vibrate. When the CO molecules slightly non-parallel to the EUV polarization, the photoemission cross-section is reduced. (b) Pump-probe spectra close to the  $4\sigma$  peak. These spectra are taken when the polarization of the EUV probe pulses is perpendicular to the platinum surface ( $p$ -polarized), and the polarization of the excitation pump pulses are parallel to the surface ( $s$ -polarized) with  $15\mu\text{J}/\text{mm}^2/\text{pulse}$  fluence. Spectra of 0 fs and 400 fs time delays are shown for comparison, showing that the the  $4\sigma$  peak in both height and area at 0 fs time delay are bigger than those at 400 fs time delay.

of the adsorbate and transfer energy to the atomic center-of-mass – causing the molecule to vibrate, or even desorb, depending on the excitation energy. For CO on Pt(111), the  $2\pi^*$  orbital is close to the Fermi-edge  $E_f$ . Hot electrons can tunnel to  $2\pi^*$  orbital to transfer energy, in a process similar to DIET/DIMET. Actually, inverse photoemission spectroscopy (IPES) has measured the  $2\pi^*$  orbital to be about 1.5 eV above the Fermi-edge for CO on Ni(111) [99], providing a channel for electronic tunneling to the CO. By fixing the polarization of the laser pulse in one particular polarization, e.g.  $p$ -polarized, as illustrated in Fig. 4.3(a), the CO molecules could start to vibrate. According to Eq. 4.5, the photoemission cross-section of a particular orbital is directly related to the overlap between the polarization of the EUV pulses and the “direction” of the wavefunction  $\phi_{i,k}$  of that orbital; or in the other words, the photoemission cross-section  $w$  of the CO  $4\sigma$  bond is a function of how well the bond lines up with the laser polarization. By using this simple idea, the oscillation period of the CO molecules can readily be measured by performing a series of pump-probe scans by following the intensity changes of the  $4\sigma$  peak.

Figure 4.3(b) shows the pump-probe spectra at time delays of 0 fs and 400 fs around the energy region of the  $4\sigma$  peak. It is clear that the  $4\sigma$  peak at 400 fs time delay is lower in both height and area when comparing to the  $4\sigma$  peak at 0 fs time delay. This change is expected because at 0 fs time delay, the CO molecular axis should still be parallel to the polarization of the EUV light, giving a maximum intensity for the  $4\sigma$  peak. At a time delay of 400 fs, the CO molecules are no longer parallel to the polarization of the EUV light, and the photoemission signal decreases accordingly.

The oscillation period of the CO molecules can be obtained by integrating the area of

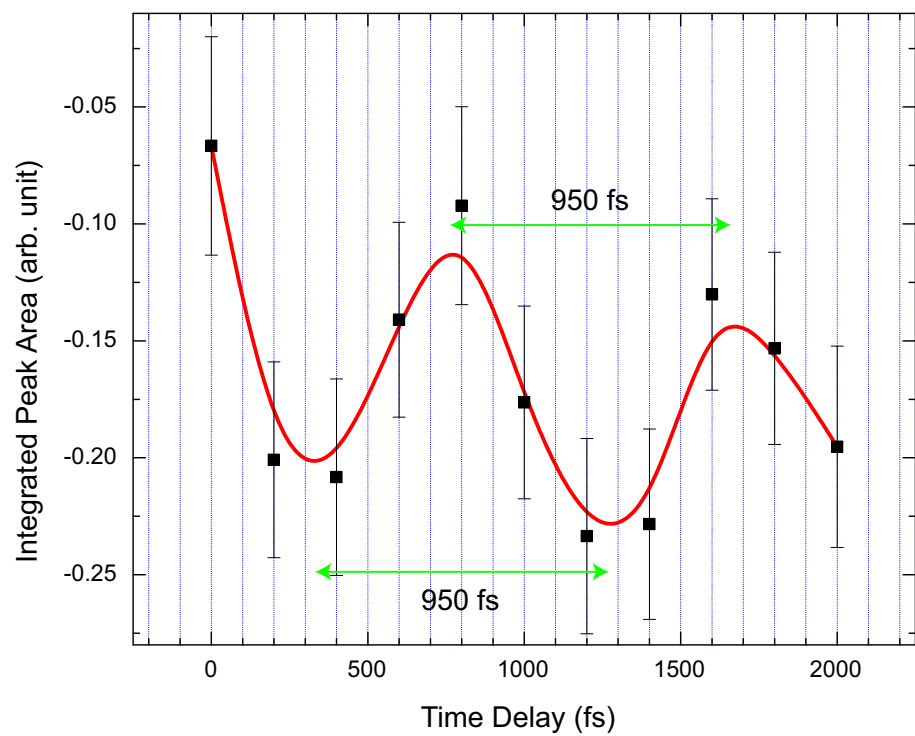


Figure 4.4: Integrated area of the  $4\sigma$  peak of the CO/Pt(111) plotted at various time delays, showing that the CO molecules are oscillating at the platinum surface after pump pulse excitation.

the  $4\sigma$  peak as a function of time delay between pump and probe. The spectra at various time delays are first subtracted from a reference spectra at -100 fs, and the remaining signals are then integrated over the binding energy of the  $4\sigma$  peak. By plotting these integrated areas versus time delay, a nice oscillatory curve is obtained, as shown in Fig. 4.4. The oscillation period is measured to be about 950 fs, when measured either at the maxima or minima of the oscillation signal. Also, in Fig. 4.4 the oscillation signal tends to decrease at longer delay times. This effect is expected since the vibrational energy of the CO molecule can slowly transfer to the platinum surface, reducing its oscillation amplitude accordingly.

Further information can be revealed at the Fermi edge. Fig. 4.5 shows the photoemission spectra at the Fermi-edge at the time delays of 0, 100, 200, and 500 fs respectively. It is obvious that the photoemission yield at 0 fs is significantly higher than for the rest of the photoemission spectra. This indicates that a significant population of non-thermal electrons are created by the pump pulse. These non-thermal electrons are still distinguishable at 100 fs, but by 200 fs, the electron distribution has cooled significantly. This is similar to our previous observation on oxygen at Pt(111) – the hot electrons distribution is significantly reduced by about 200 fs.

## 4.4 Discussion

### 4.4.1 CO normal modes on a platinum surface

In the gas phase, a molecule can have  $3N$  degrees of freedom, which can be divided into three translational, 3 rotational and  $3N - 6$  vibrational modes (for linear molecules, 2 rotational and  $3N - 5$  vibrational modes).  $N$  is the number of atoms in the molecules.

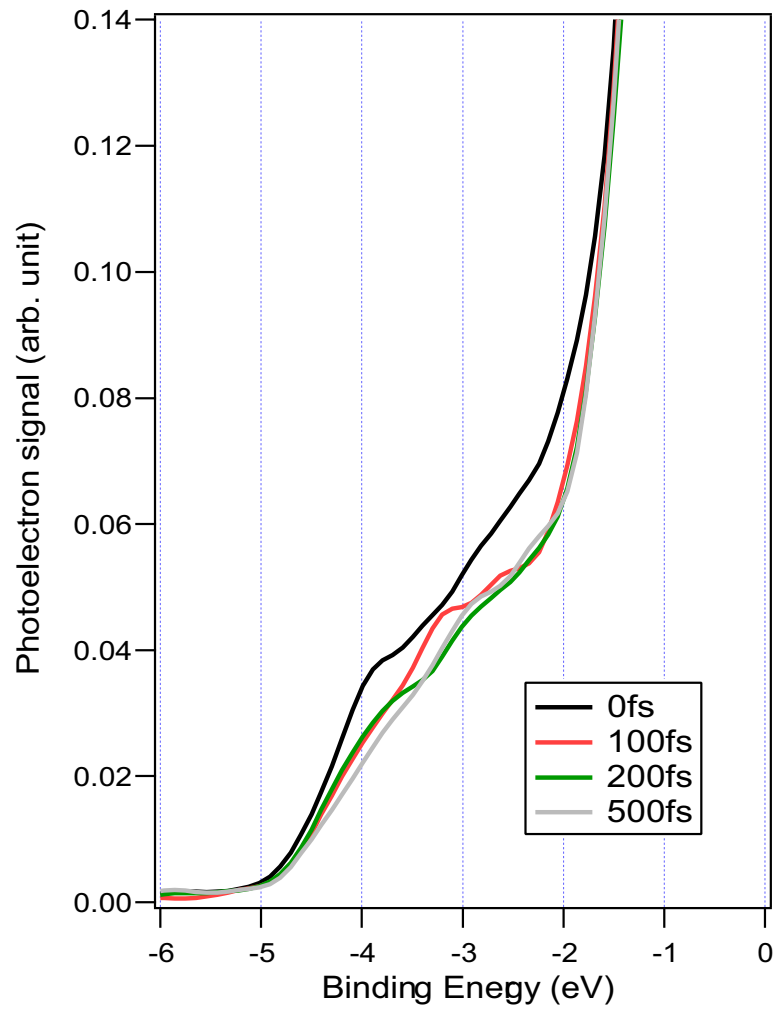


Figure 4.5: Pump-probe spectra near the Fermi-edge, showing that hot electrons are rapidly excited when the ultrafast pump pulses excites the surface. They subsequently relax in about 200 fs. There is a static component resulting from a small residual 29<sup>th</sup> harmonic.

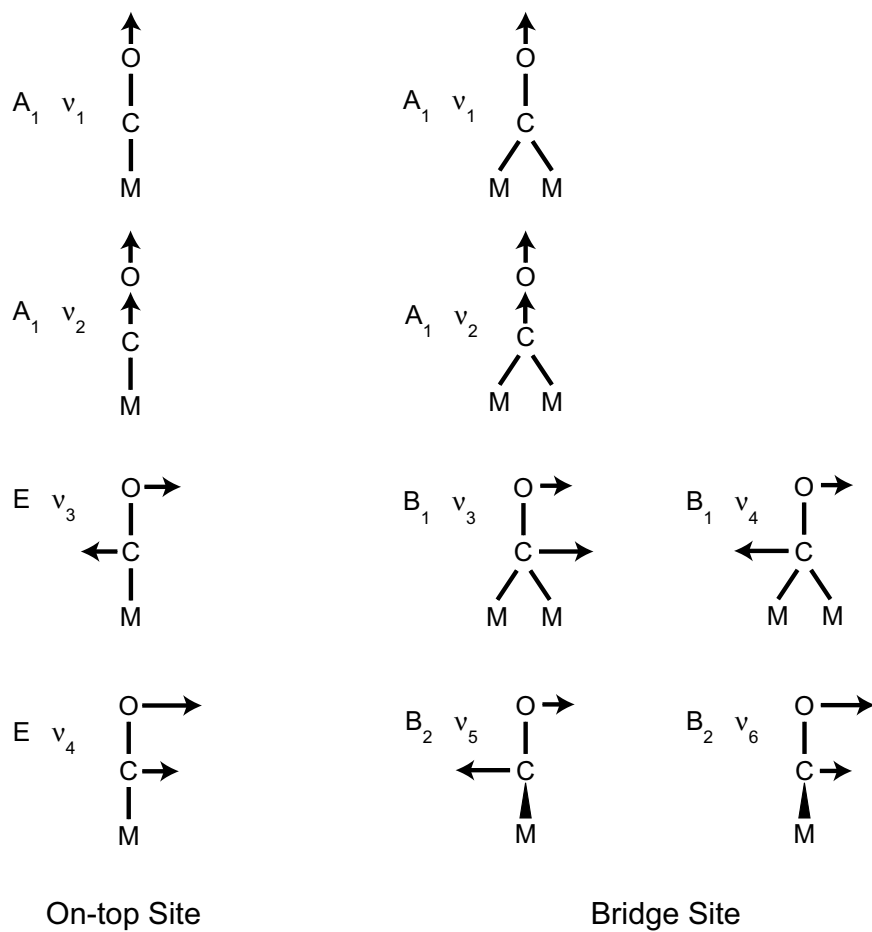


Figure 4.6: Schematic representation of the normal modes of on-top and bridge-bonded CO on platinum surface. The relative length of the arrows represent the movements of the carbon and oxygen atoms. (figure adapted from Ref. [100] and Ref. [101])

When molecules adsorb on surfaces, all translational and rotational motions are restricted, so the  $3N$  degrees of freedom are all vibrational modes. These vibrational modes are best classified as 3 frustrated translations, in which the molecule, as a whole, moves perpendicular or parallel to the surface, 3 (2 for a linear molecule) frustrated rotations, and finally  $3N - 6$  ( $3N - 5$  for linear molecule) vibrational modes.

For classification purposes, point group symmetry can be used to associate the CO adsorption to the top site and the bridge site on the platinum surface. The top site gives the  $C_{4v}$  point group, and the bridge site gives  $C_{2v}$  point group. Fig. 4.6 shows schematically the form of localized vibrational modes for CO on Pt(111) on the on-top and bridging position. In each case, there are two modes belonging to the totally symmetric  $A_1$  representation, which have their dipole moment changes normal to the surface. Hence,  $\nu_1$  is closely related to the free molecule C-O stretching mode.  $\nu_2$  is a hindered translation mode normal to the platinum surface, which becomes essentially a Pt-C stretching mode. The remaining four modes – the  $x$  and  $y$  frustrated translations and the frustrated rotations appear as degenerate pairs for the top site CO molecules; but in the bridge site, the degeneracy is lifted and results in two modes,  $\nu_3$  and  $\nu_4$ , in the plane of the bridge site, and two modes,  $\nu_5$  and  $\nu_6$ , perpendicular to the plane of the bridge site.

These vibrational modes can be measured using energy loss methods. In general, infrared spectroscopy (IRS) and electron energy loss spectroscopy (EELS) have been employed successfully for measuring adsorbate vibrational frequencies with energies above  $200 \text{ cm}^{-1}$  [102, 103]. For vibrational energy lower than this range, a helium atom scattering technique is employed to investigate the low frequency modes [104, 105, 101]. In

	normal mode energy (cm <sup>-1</sup> )		oscillation period (fs)	
	on-top site	bridge site	on-top site	bridge site
C-O stretch $\nu_1$	2100	1871	16	18
Pt-CO stretch $\nu_2$	480	361	72	92
CO frustrated rotation $\nu_3$		411 *		81
CO frustrated translation $\nu_4$	48	59	696	566

Table 4.3: Normal mode energies of CO adsorbed on Pt(111) (\* calculated for CO/Ni)

particular, for CO adsorbed on Pt(111) at a low coverage of CO ( $\leq 1/3$  mono-layer), CO molecules mainly occupied on the on-top sites. The high frequency C-O stretching mode  $\nu_1$  is measured to be 2100 cm<sup>-1</sup>(258 meV), and the Pt-C stretching mode  $\nu_2$  is at a relatively lower frequency, estimated to be 480 cm<sup>-1</sup>(58 meV) by EELS [75, 106]. When the CO coverage increases to 0.5 mono-layer and above, the bridge sites will start to be filled by the CO molecules. Therefore, the EELS spectrum will start to develop two new additional loss peaks at slightly reduced energies at 1871 cm<sup>-1</sup> (232 meV) and 361 cm<sup>-1</sup> (45 meV), corresponding to the C-O stretching mode and the Pt-C stretching mode at the bridge sites respectively. The CO frustrated rotation mode  $\nu_3$  has been calculated for CO adsorbed on Ni, and the calculated value is 411 cm<sup>-1</sup> (51 meV), which is in the same order of magnitude as the  $\nu_2$  mode. (For the other two modes calculated for CO/Ni:  $\nu_1 = 2088$  cm<sup>-1</sup> (259 meV), and  $\nu_2 = 437$  cm<sup>-1</sup> (54 meV). These are similar to the measured value of CO adsorbed on Pt, and hence, it is reasonable to believe that the  $\nu_3$  of CO/Pt(111) has a similar value) [100]. Finally, for the frustrated translation mode  $\nu_4$ , helium scattering experiment measured the value to be 48 cm<sup>-1</sup> (6 meV) for the top site, and 59 cm<sup>-1</sup> (7 meV) to the bridge site [101, 107].

The oscillation periods of these modes can be calculated from the measured energies. Assuming that all normal modes of the adsorbates are harmonic oscillators, then the vi-

brational energies can be written as

$$E_n = \left(n + \frac{1}{2}\right)\hbar\omega \quad (4.8)$$

where  $n$  is the quantum number of the normal mode, and  $\omega = 2\pi/\tau$  is the angular frequency, and  $\tau$  is the oscillation period. For energy loss experiments, the measured energy is the energy difference between the ground state ( $v = 0$ ) and the excitation state ( $v = 1$ ), and hence, the vibrational period can be converted from the measured energy by

$$\tau = h/E_{measured} \quad (4.9)$$

The energies of the four normal modes of the the CO/Pt(111) and their corresponding converted oscillation periods are tabulated in Table 4.3.

Considering all of the vibrational modes of CO/Pt(111), the oscillation period corresponding to the frustrated translation mode  $\nu_4$  ( $\tau_4 = 696$  and  $566$  fs) is the closest one to the period we measured using TR-UPS ( $\tau_{\text{TR-UPS}} \simeq 950$  fs). All the other mode periods are more than an order of magnitude shorter in time than the period measured. In fact, the frustrated translation mode  $\nu_4$  and the frustrated rotation mode  $\nu_3$  should be most sensitive to the polarization of the EUV pulses, due to the fact that these modes directly affect the orientation of CO molecules on the platinum surface, and subsequently affect the orientation of the  $4\sigma$  orbital. For the frustrated rotation mode  $\nu_3$ , one would expect another oscillation period on the order of 100 fs should be observed and that this fast period should be superimposed on the slow varying oscillation period of  $\nu_4$ . However, preliminary study of measuring the variation of the  $4\sigma$  peak with a finer time resolution does not reveal another oscillation feature, indicating the possibility that the  $\nu_3$  mode might not be as easily

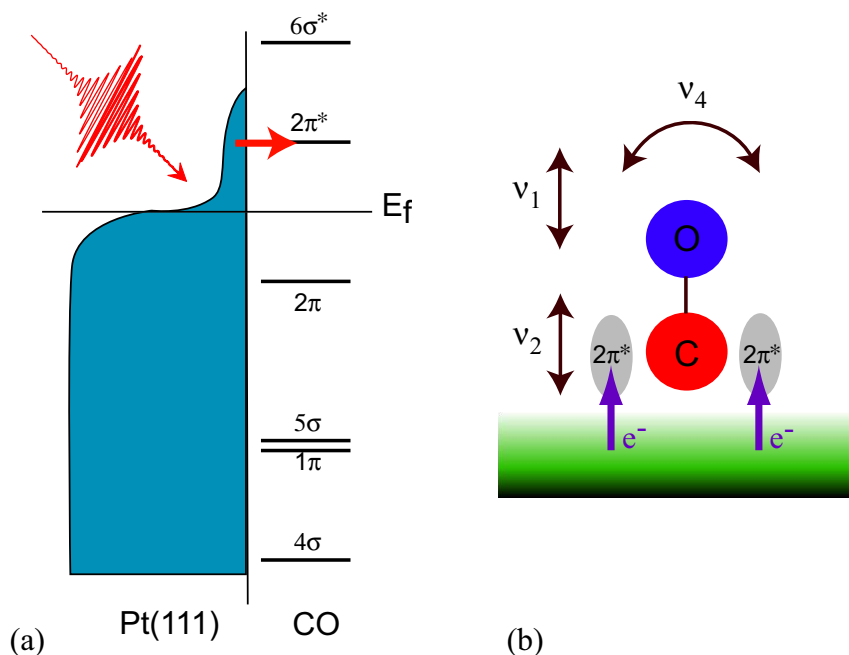


Figure 4.7: (a) When an ultrafast pulse excites the platinum surface, hot electrons are created on the surface. The hot electrons then tunnel to the  $2\pi^*$  orbital of the CO molecule. (b) Due to the bonding character to the platinum surface of the  $2\pi^*$  orbital, the C-O vibrational mode  $\nu_1$  and the CO-Pt vibrational mode  $\nu_2$  will be induced. The frustrated translation mode  $\nu_4$  could either be directly excited by the hot electron, or subsequently excited due to energy coupling between modes.

excited as the frustrated translation  $\nu_4$ . In fact, in energy loss spectroscopy, in our knowledge, the  $\nu_3$  mode has not been observed experimentally. This might be an indication that the potential energy surface of the CO/Pt(111) system might prohibit the excitation of the CO frustrated rotation mode  $\nu_3$  effectively.

#### 4.4.2 Hot electrons mediated excitation

The excitation mechanism of the  $\nu_4$  mode related to hot surface electrons that are created and sustained within the first 200 fs after pump pulse excitation. As shown in Fig. 4.4, the oscillation begins immediately after pump pulse excitation, and the  $4\sigma$  orbital reduces its intensity significantly by a 200 fs time delay. According to the two temperature model

discussed in the last chapter, the surface electrons respond to ultrafast pulse excitation almost instantaneously through directly adsorbing the ultrafast pulse energy which could subsequently raises the electron temperature to several thousand Kelvin, depending on the pump pulse intensity and pulse-width. However, the surface lattice cannot directly respond to the ultrafast pulse excitation, and remains relatively “cold” for picoseconds. If the CO excitation is phonon-mediated, as in conventional surface chemistry, a time delay of picoseconds would be expected before the onset of oscillation. Therefore, once again, the hot surface electrons created by ultrafast pulses play an important role in the CO excitation observed.

For CO on Pt(111), the unoccupied  $2\pi^*$  orbital is close to the Fermi-level. Since the photon energy of our pump pulse is 1.5 eV, the hot surface electrons will be excited to 1.5 eV above the Fermi-edge. Therefore, these hot electrons will have sufficient energy to reach this unoccupied CO orbital through tunneling, as shown in Fig. 4.7. In fact, the  $2\pi^*$  orbital is an anti-bonding orbital with respect to the bonding between carbon and oxygen atom; on the other hand, occupying the  $2\pi^*$  orbital would enhance the bonding strength between the platinum surface and the CO molecule.

Therefore, after the hot surface electron transfers to the  $2\pi^*$  orbital of the CO molecules, the potential energy surface (PES) of the CO molecules is suddenly excited through Franck-Condon excitation. The nuclei of the CO molecules are not positioned at the energy minimum of the excited PES, and the nuclei will be driven along the excited PES to new positions. Therefore, the distance between the carbon atom and the oxygen atom will be increased, and the distance between the CO molecule and the platinum surface will be-

come shorter. Typically, these hot electrons will only stay on the adsorbates for a time scale of about 10 fs, as discussed in the studies of unoccupied state lifetime of adsorbates using two-photon photoemission techniques from Sec. 1.3. After the hot electrons leave the  $2\pi^*$  orbital of the CO, the PES will be relaxed to the ground-state, and the carbon and oxygen atoms are now required to reverse their courses. Because of these motions, the energy of the hot electrons is partly transferred to kinetic energy of the nuclei. Hence electron transition processes result in launching vibrations for two normal modes  $\nu_1$  and  $\nu_2$ . This picture is very similar to the DIET/DIMET process of desorption by ultrafast pulse. Hot surface electrons transfer energy to molecular motion through the excited potential energy surface by Franck-Condon excitation, as discussed in the appendix.

The excitation of the frustrated translation mode  $\nu_4$  could be due to subsequent mode coupling between the highly excited modes  $\nu_1$  and  $\nu_2$  with  $\nu_4$ , or could be due to direct excitation by the hot surface electrons, or even a mix of the two mechanisms. If the former is true, then the coupling time between the normal modes should be fairly “fast” in order to explain the quick onset of the observed oscillation signal. Further investigation on this process will be needed in order to fully understand the excitation mechanism of the  $\nu_4$  mode.

Finally, the oscillation period we measured using TR-UPS is about 950 fs, which is longer than the numbers measured by helium atom scattering experiments (696 and 566 fs). In fact, for the technique of time-resolved vibrational sum-frequency generation, as discussed in Sec. 1.5.2, a strong transient redshift of the vibrational energy for the C-O stretch mode has been observed after ultrafast pulse excitation, . The vibrational energy

is shifted from  $\sim 2020 \text{ cm}^{-1}$  to  $\sim 1980 \text{ cm}^{-1}$  and persists for more than 20 ps, as shown in Fig. 1.10(b). They explained this effect is caused by anharmonic coupling of the C-O stretch mode to low-frequency frustrated modes [36, 35, 108, 109]. Further investigation is needed to clarify how this energy redshift happens.

## 4.5 Conclusion

In this chapter, measuring the vibrational period of an adsorbate in the time domain has been demonstrated using the symmetry of the molecular orbitals and the polarization of the EUV ultrafast pulses. In particular, the CO frustrated translation mode  $\nu_4$  is measured to be about 950 fs, similar to results obtained using helium scattering techniques in the energy domain. Actually, CO translational motion has been proposed to be very important to the CO oxidation process on metal surfaces, as well as the rotational motions of the  $\text{O}_2$  molecules, as reported in the last chapter. Density functional calculations [68, 110, 103] have suggested that in the beginning of the CO oxidation process, oxygen molecules rotate from the bridge site to the hollow site in order to elongate the intermolecular bond between the two oxygen atoms. This results in dissociation into two oxygen atoms with lower dissociation energy. Simultaneously, CO molecules translate and bend towards the oxygen molecules (or atoms) to “attract” one of the oxygen atoms to recombine with it and finally leave the surface as  $\text{CO}_2$ . If this picture of CO oxidation is correct, then the two measurements that we performed of  $\text{O}_2/\text{Pt}(111)$  and  $\text{CO}/\text{Pt}(111)$  support observation of the first steps in the suspected mechanism of CO oxidation.